Applied Physics Letters ARTICLE scitation.org/journal/apl

Focus of ultrasonic underwater sound with 3D printed phononic crystal

Cite as: Appl. Phys. Lett. **119**, 073501 (2021); doi: 10.1063/5.0058415
Submitted: 29 May 2021 · Accepted: 1 August 2021 ·
Published Online: 16 August 2021

Zhaoxi Li,[1] Shenghui Yang,[1] Danfeng Wang,[2] Han Shan,[2] Dongdong Chen,[1] Chunlong Fei,[1,a)] Meng Xiao,[3,a)] and Yintang Yang[1]

AFFILIATIONS

[1]School of Microelectronics, Xidian University, Xi'an 710071, China
[2]School of Central South University, Changsha Hunan 410083, China
[3]Key Laboratory of Artificial Micro- and Nano-Structures of Ministry of Education and School of Physics and Technology, Wuhan University, Wuhan 430072, China

[a)]**Authors to whom correspondence should be addressed:** clfei@xidian.edu.cn and phmxiao@whu.edu.cn

ABSTRACT

Ultrasound is widely used in various applications, ranging from ultrasound imaging to particle manipulation. Acoustic materials, such as phononic crystal (PC) and metamaterials, are designed to control the propagation and concentration of ultrasound. While traditional metal-based underwater PCs are usually limited to large 2D structures and used for low-frequency sound wave manipulation, it is difficult to reach the ultrasonic frequency region of the order of 1 MHz with cumbersome metallic structures. Here, in this work, we proposed a 3D printed gradient-index phononic crystal (GRIN PC) lens based on the hyperbolic secant index profile. With a huge impedance difference between air and the 3D printing materials, the GRIN PC lens adhered to the ultrasonic transducers can easily manipulate the propagation of acoustic waves and achieve wave focusing. This transparent and flat lens demonstrates the beam focusing in water even at a high frequency. The integration and miniaturization of transducer and lens make particle capture convenient in relevant medical applications.

Ultrasound is widely used in biology, chemistry, and industrial applications, such as ultrasound imaging,[1] nondestructive testing,[2] and cell and particle manipulation.[3,4] The manipulation of ultrasonic waves, such as focusing, can help to improve the capability of biomedical imaging, achieve acoustic tweezers functionality, and lead to other potential applications.[5,6] Focusing of ultrasound has been realized with self-focusing mechanisms, phased array transducers, and acoustic lenses. Self-focusing mechanisms are usually based on nonlinear effects, which already require large sound intensity itself.[7] Compared with phase array transducers, acoustic lenses are much cheaper and more efficient. The existing focusing acoustic lenses mainly include curved solid lenses, Fresnel lenses,[8,9] acoustic liquid lenses,[10,11] and acoustic metamaterials and metasurfaces.[12–14] In general, curved solid lenses are bulky and difficult to manufacture precisely. Acoustic metamaterials and metasurfaces have achieved great success in air-borne sound wave manipulations, including sound wave focusing with the help of 3D printing technology.[15–17] However, it is difficult to directly implement such an approach for underwater sound due to the small impedance difference between 3D printed materials and water. Wu *et al.*[14] reported a metallic metasurface for focusing ultrasonic waves underwater at 500 kHz; however, this metasurface worked in the reflection mode, which was difficult to integrate with the ultrasonic sound sources for applications. Although acoustic liquid lenses exhibit the advantages of adjustable focus and good impedance matching output performance, the unstable surface shapes of them limit their applications.[18]

During the last few decades, the rapid development of the phononic crystal (PC) has successfully expanded the capability of acoustic materials.[19–28] The effective refractive index of PCs can be smoothly altered by changing the constituent materials or the structure, which, thus, leads to the emergence of gradient-index phononic crystals (GRIN PCs). GRIN PCs have also been used in the focusing of sound waves, including both Rayleigh waves[29] and Lamb waves.[30] For underwater acoustics, PCs are mainly constructed using metals that exhibit acoustic impedances quite different from water. However, it remains challenging to fabricate complex 3D metallic PCs. Currently, the vast majority of research for underwater sound wave manipulation is still limited to large 2D structures[31] and is valid only for low-frequency.[32–34]

In this work, we report a high-frequency GRIN PC lens for underwater acoustic focusing based on the hyperbolic secant index

profile.[35] To introduce the impedance contrast, our lens consists of a 3D-printed polymer as the background and air as the contrasting inclusion. Similar ideas of introducing ultralow impedance constituents underwater have also been discussed with GRIN PCs,[33] Fresnel zone plate lenses,[32] and soft gradient-index metasurfaces[34] at frequencies around the order of 0.1 MHz. Our design works at a much higher frequency at around 1 MHz. Meanwhile, we note that the finite distances between the sound sources and the focus lenses in Refs. 32 and 33 are obstacles for device integration. In contrast, the GRIN PC lens herein has a simple structure and is compact such that it can be directly integrated with the ultrasonic transducers (also can be disassembled from the transducers and redesigned for other functionalities). Jin *et al.*[34] considered metasurfaces that can be deposited on sound sources by spatially assembling different units with a controlled porosity of silicone rubber. Our approach, in comparison, is more flexible and compatible with commercial 3D printers and with unprecedented precision at the sub-millimeter level. Those merits of our approach discussed above facilitate the integration and miniaturization

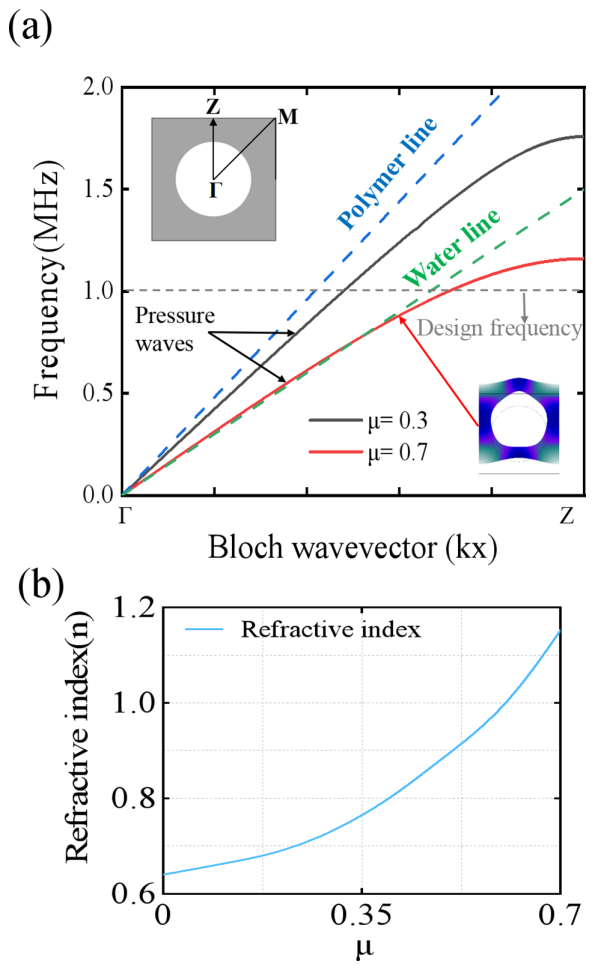

FIG. 1. (a) Band structure of the proposed PC for different scaling factor (μ) along Γ-Z. (b) Relationship between the effective refractive index of PCs and the scaling factor (μ) at 1 MHz.

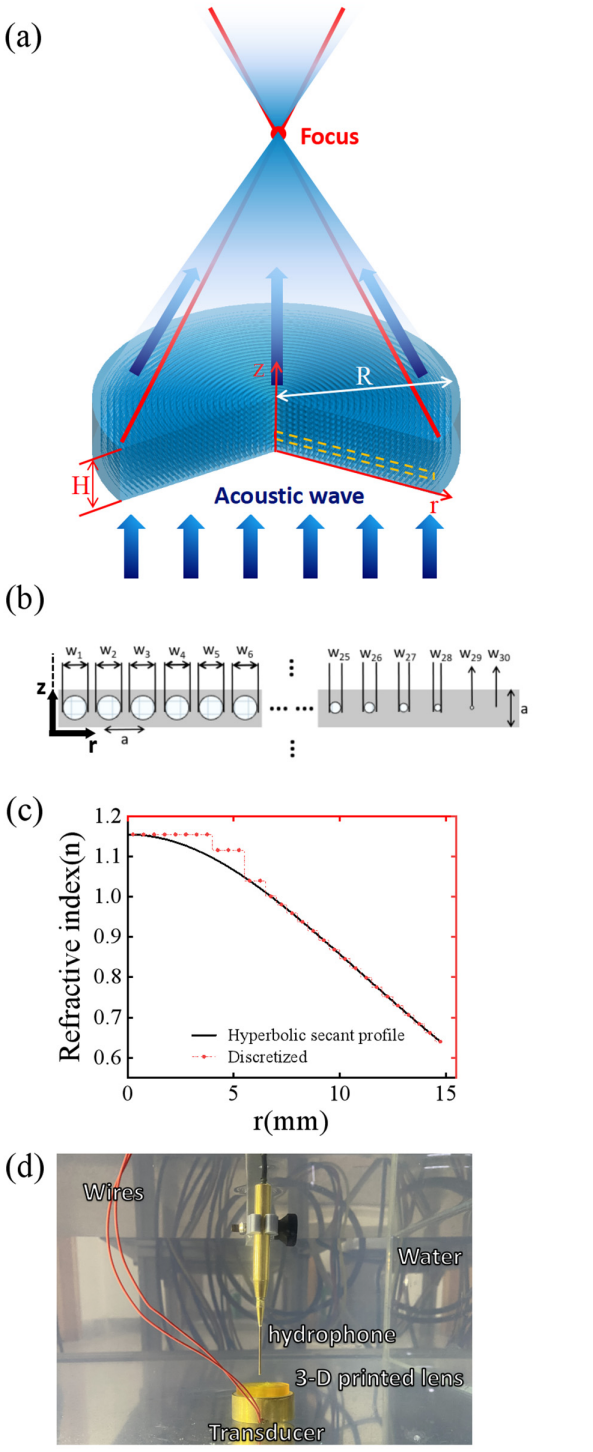

FIG. 2. (a) The structure of the proposed GRIN PC lens for ultrasonic focusing. (b) The structure of a cross sectional plane of the toroidal scatterers. (c) The desired hyperbolic secant index profile for a focus lens (black line) and the corresponding discretized GRIN PC implementation (red points). (d) Photograph of the experimental setup.

of transducers and lenses, which then brings a big leap forward in medical applications, such as particle capture, imaging, and neuromodulation.[36–38] In our work, both simulations and experiments show the focusing effect of the GRIN PC, and the results are in good agreement.

We start with a 2D unit cell composed of an air hole (white) inside a square polymer matrix (gray), as shown in the upper left inset of Fig. 1. We assume that the sound wave generated by the transducer is predominantly longitudinal wave and the mixture of longitudinal wave and transverse wave in GRIN lens is negligibly small (which is true when index change along the transverse direction is smooth); hence, the excitation of transverse mode is ignored for simplicity. Meanwhile, the sound wave propagating inside the lens is approximated to be only along the Γ-Z direction, and thus, the effective refractive index along this direction is used to calibrate the phase delay inside the PC. Figure 1(a) shows the band structure for two scaling factors ($\mu = W/a$, defined as the ratio between the diameter W of the air chamber and the lattice constant a, where $a = 0.5$ mm), $\rho_{\text{polymer}} = 1300\ \text{kg/m}^3$, velocities of the P-wave $c_p = 2400$ m/s, and the S-wave $c_s = 1000$ m/s in polymer (measured experimentally for the printing polymer). The numerical simulations in this work are all performed with a commercial finite element software COMSOL[36] (see details in the supplementary material, Sec. I). The green and blue lines represent the waterline and polymer line for reference. The smaller μ is, the smaller the effective refractive index eventually approaches the polymer line. The inset at the lower right shows the amplitude of displacement field at $\mu = 0.7$ and 1 MHz, wherein we can see the longitudinal feature. The designed frequency in our work is set at 1 MHz as marked by the gray dashed line in Fig. 1(a) at which the dispersion of bands is still relatively small.

The phase velocity of the longitudinal mode is defined as $c_p = 2\pi f/k_x$, where $f = 1$ MHz and k_x is the Bloch wave vector. The effective refractive index of the GRIN PC relative to water is $n = c_w/c_p$, where $c_w = 1500$ m/s is the speed of sound in water. Figure 1(a) shows that when the frequency stays at 1 MHz, as μ increases, n increases, as shown in Fig. 1(b). To be more specific, from $n = 0.64$ for $\mu = 0$ to $n = 1.155$ for $\mu = 0.7$. The dependence of refractive index on μ then offers us the capability to design an acoustic focus lens. A GRIN PC lens was designed based on the hyperbolic secant index profile, which is defined as

$$\mathrm{n}(r) = n_o \operatorname{sech}\ \mathrm{R}(\alpha r). \tag{1}$$

Here, $n_0 = n(r = 0)$ is the refractive index on the z-axis, r represents the distance from the center of the lens, and α is the gradient coefficient defined as

$$\alpha = \frac{1}{\mathrm{R}} \cosh^{-1}\left(\frac{n_0}{n_1}\right). \tag{2}$$

In our case, $R = 15$ mm is the radius of the GRIN PC lens. From Eq. (1), we can see that the refractive index is maximum at the center and minimum at the periphery, and thus, the GRIN PC can work as a focus lens as schematically shown in Fig. 2(a). Here, the acoustic waves incident from the lower side and focus after propagating some distance. For a large enough lens, the focal length of the lens is given by[39]

$$d = \frac{1}{n_1 \alpha \sin(\alpha H)}, \tag{3}$$

where H is the thickness of the lens.

To achieve the refractive index distribution as defined in Eq. (1), the GRIN PC in our case consists of 10 identical layers with a total thickness of $H = 5$ mm. Each layer consists of 30 concentric torus air holes with equally spaced major radii and different minor radii. The cross section of one layer as marked by the yellow dashed rectangular in Fig. 2(a) is shown in Fig. 2(b). The major radii are chosen to be ma, where m is an integer and a is the lattice constant same as Fig. 1(a). Thus, the radius of the GRIN PC is $R = 15$ mm. In principle, the minor radius of each torus air can be independently designed. In our case, we consider the propagating of the acoustic wave along the z-direction and assume that there is no phase variation in the transverse direction. Under such a condition, the effective refractive index of each annulus is the same as that of the 2D unit cell defined in Fig. 1(a). Hence, we can approximate the hyperbolic secant profile defined in Eq. (1) with a discretized distribution of W as shown in Fig. 2(c), where the black line shows the refractive index distribution as a function of r with $n_1 = 1.155$ and $n_0 = 0.64$. The specific values W of all 30 tori are listed in Table I. Note here, the discretization of a few tori at the center is not smooth due to the consideration of the printing precision. As will be shown later, the effect is negligibly small.

The experimental setup and the structure of the 3D printed GRIN PC lens are shown in Figs. 2(d). The lens is made up of photosensitive resin and fabricated with a 3D printer (NanoArch S140) with a precision of 50 μm. (Details of the printing process are provided in the supplementary material.) The printed lens is placed on the surface of the ultrasonic transducer using a thin layer of ultrasound transmission gel, which gives good acoustic coupling and temporary mechanical fixing. During the experiments, the transducer was excited with a 10-cycle sine wave at 1 MHz by a signal generator (SMB100A, Rohde & Schwarz, GER) and amplified by a 26 dB power wideband amplifier (A TA-122D, Aigtek, CHN). A hydrophone (NH1000, PA, UK) with a lateral step size of 300 μm and an axial step size of 300 μm was used to scan the pressure field in a rectangular region [defined in Fig. 3(a)] with the dimensions of $30 \times 60\ \text{mm}^2$ (yz-plane). The hydrophone was controlled by a homemade multi-functional ultrasonic test platform based on the LabVIEW software.

TABLE I. The diameter W of the internal spherical air chamber of each unit cells.

	W1∼W8		W9	W10	W11	W12	W13	W14	W15	W16	W17	W18
Diameter (mm)	0.35		0.3375	0.3375	0.3375	0.325	0.325	0.3125	0.3	0.2875	0.275	0.2625
	W19	W20	W21	W22	W23	W24	W25	W26	W27	W28	W29	W30
Diameter (mm)	0.25	0.2375	0.225	0.2125	0.2	0.175	0.1625	0.15	0.125	0.1	0.05	0

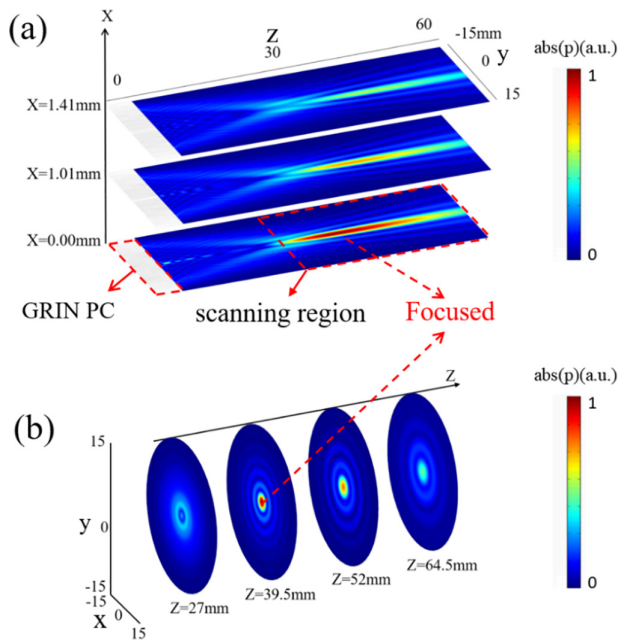

FIG. 3. (a) and (b) Simulations of normalized absolute sound pressure (a.u.) distributions on a few typical *yz*- (a) and *xy*-planes (b). A ultrasonic transducer is operated at 1 MHz with the designed GRIN PC Lens attached to it on the positive *z* side.

Figures 3(a) and 3(b) show the simulated normalized absolute sound pressure distributions on a few typical *yz*- and *xy*-planes. The proposed GRIN PC lens can focus acoustic waves with a focal length around $f = 39.5$ mm. Meanwhile, the focusing is rotational symmetric since the whole system is rotationally invariant.

Figures 4(a) and 4(b) show the comparison between the (a) simulated and (b) measured underwater pressure fields and are normalized to the maximum of each of those plots. Figure 4(c) shows the pressure field without GRIN PC lens for reference where no obvious focusing effect is seen. Figure 4(c) is normalized to the maximum in Fig. 4(b). Figures 4(d) and 4(e) show the normalized pressure amplitude through the focal spot along with the lateral and vertical directions, respectively. Obviously, the signal amplitude with the GRIN PC lens is larger than that without the lens. Measured (simulated) pressure distribution gives a horizontal resolution (at −6dB) of 2.7 mm (2.8 mm), a vertical resolution (at −3dB) of 22.8 mm (22.4 mm), and the focal point at $z = 39.0$ mm and $y = 0.0$ mm ($z = 39.0$ mm and $y = 0.0$ mm). Both resolution and focal point experimentally obtained are in good agreement with those from the simulation. The subtle difference may come from fabrication imperfection, and shear waves are ignored in both the design and simulation.

Though the GRIN PC here is designed with a designed frequency of 1 MHz, it works for relatively broadband with a slight shift of the focus points. Figure 5(a) gives the peak amplitude of voltage measured at different excitation frequencies at the focal spot. The voltage enhancement reaches the maximum value at 1 MHz while exhibits a pretty broadband enhancement frequency range. To verify the

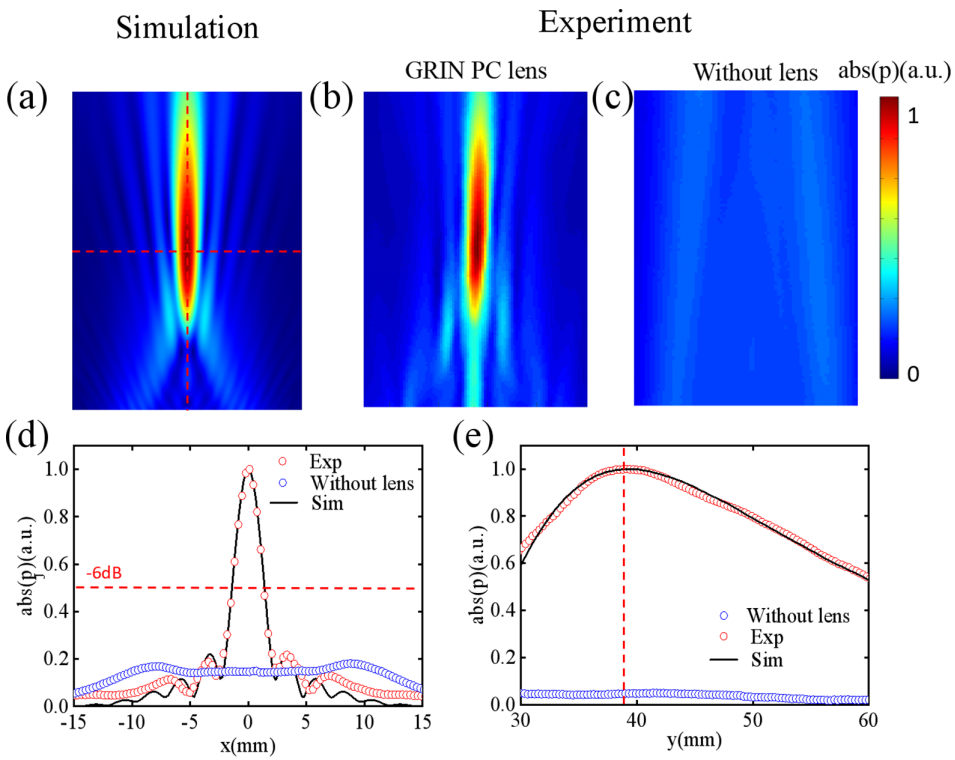

FIG. 4. (a)–(c) The distribution of underwater pressure fields for (a) simulation, (b) measured with lens, and (c) without lens. The plots are normalized by the corresponding maximum values in (a) and (b), and the plot in (c) is normalized by the maximum of b before normalization. (d) and (e) Profiles of normalized pressure amplitude through the focal spot along the lateral (d) and vertical (e) directions.

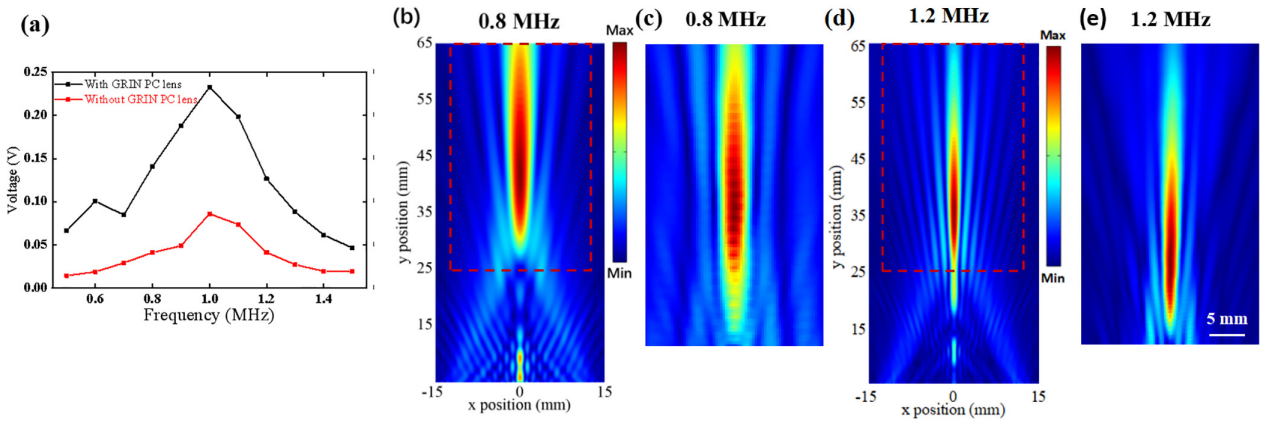

FIG. 5. (a) The peak amplitude of voltage measured at different excitation frequencies at the focal spot. The distributions of simulated [(b) and (d)] and measured [(c) and (e)] normalized pressure fields with the presence of the GRIN PC lens in the xz-plane at [(b) and (c)] f = 0.8 MHz and [(d) and (e)] f = 1.2 MHz.

broadband focusing effect, the transducer was excited at frequencies f = 0.8 MHz and f = 1.2 MHz. A hydrophone (NH1000, PA, UK) was used to scan the pressure field in a rectangular region (marked by red dotted line in Fig. 5) with the dimensions of $25 \times 40\ \text{mm}^2$ (*yz*-plane). The simulated and measured normalized pressure fields with GRIN PC at these two representative frequencies are provided in Figs. 5(b)–5(e), where we can see clear and consistent focusing effect.

In this work, we designed a high-frequency and ultra-compact 3D printed GRIN PC lens based on the hyperbolic secant index profile and verified the 3D focusing effect underwater. The good agreement between simulations and the experiments validates the effectiveness of the GRIN PC lens. Moreover, the proposed PC lens has a simple structure and can be directly adhered to the surface of an ultrasonic transducer and, thus, is suitable in various situations and has a great potential in underwater applications. We note that by introducing air into the phononic crystals, the transmission efficiency of the transducer may decrease a little bit due to the impedance mismatch. This drawback can be further reduced by gradually varying the parameters of layers along the *z*-direction (easy to be implemented with the current 3D printing technique) to smooth the impedance variation. With the combination of photosensitive resin and air through the 3D printing technique, our work points to the possibility of arbitrary controlling wavefront in terms of both amplitude and phase for ultrasonic application.

See the supplementary material for details of numerical simulations and fabrication of the 3D printed GRIN PC lens.

Financial support from the National Natural Science Foundations of China (Nos. 61974110 and 11904264), the Natural Science Foundations of Shaanxi Province (No. 2020JM-205), the Shaanxi Provincial Association of Science and Technology Young Talents Support Project (No. 20190105), and the National Key Research and Development Program of China (No. 2017YFC0109703) is greatly appreciated.

DATA AVAILABILITY

The data that support the findings of this study are available from the corresponding authors upon reasonable request.

REFERENCES

[1]B. P. Zhu, D. W. Wu, Y. Zhang, J. Ou-Yang, S. Chen, and X. F. Yang, Ceram. Int. **39**, 8709–8714 (2013).
[2]X. Sun, C. Fei, Q. Chen, D. Li, Z. Tang, J. Zhuang, Y. Wu, J. Chen, R. Wu, and Y. Tang, J Mater. Sci.: Mater. Electron. **31**, 1839–1845 (2020).
[3]A. Ozcelik, J. Rufo, F. Guo, Y. Gu, P. Li, J. Lata, and T. Huang, Nat. Methods **15**, 1021–1028 (2018).
[4]C. Fei, Y. Li, B. Zhu, C. Chiu, Z. Chen, D. Li, Y. Yang, K. K. Shung, and Q. Zhou, Appl. Phys. Lett. **109**, 173509 (2016).
[5]M. Baudoin, J. L. Thomas, R. Al Sahely, J. C. Gerbedoen, Z. Gong, A. Sivery, and A. Vlandas, Nat. Commun. **11**, 4244 (2020).
[6]C. Fei, C. T. Chiu, X. Chen, Z. Chen, J. Ma, B. Zhu, and Q. Zhou, Sci. Rep. **6**, 28360 (2016).
[7]Q. F. Zhou, C. Sharp, J. M. Cannata, K. K. Shung, G. H. Feng, and E. S. Kim, Appl. Phys. Lett. **90**, 113502 (2007).
[8]S. A. Farnow and B. A. Auld, Appl. Phys. Lett. **25**, 681 (1974).
[9]M. Molerón, M. Serra-Garcia, and C. Daraio, Appl. Phys. Lett. **105**, 114109 (2014).
[10]Z. Li, R. Guo, D. Chen, C. Fei, X. Yang, D. Li, C. Zheng, J. Chen, R. Wu, W. Feng, Z. Xu, and Y. Yang, IEEE Trans. Ultrason. Ferroelectr. Freq. Control **68**, 1546–1554 (2021).
[11]Z. Li, R. Guo, C. Fei, D. Li, D. Chen, C. Zheng, R. Wu, W. Feng, and Y. Yang, Appl. Acoust. **175**, 107787 (2021).
[12]S. A. Cummer, J. Christensen, and A. Alù, Nat. Rev. Mater. **1**, 16001 (2016).
[13]N. Kaina, F. Lemoult, M. Fink, and G. Lerosey, Nature **525**, 77–81 (2015).
[14]X. Wu, X. Xia, J. Tian, Z. Liu, and W. Wen, Appl. Phys. Lett. **108**, 163502 (2016).
[15]Y. Li, G. Yu, B. Liang, X. Zou, G. Li, S. Cheng, and J. Cheng, Sci. Rep. **4**, 6830 (2015).
[16]Y. Li, X. Jiang, R. Q. Li, B. Liang, X. Y. Zou, L. L. Yin, and J. C. Cheng, Phys. Rev. Appl. A. **2**, 064002 (2014).
[17]Y. Ding, E. C. Statharas, K. Yao, and M. A. Hong, Appl. Phys. Lett. **110**, 241903 (2017).
[18]C. Song, L. Xi, and H. Jiang, J. Appl. Phys. **114**, 194703 (2013).
[19]N. Bachelard, C. Ropp, M. Dubois, R. Zhao, Y. Wang, and X. Zhang, Nat. Mater. **16**, 808–813 (2017).
[20]O. Bou Matar, J. F. Robillard, J. O. Vasseur, A. C. Hladky-Hennion, P. A. Deymier, P. Pernod, and V. Preobrazhensky, J. Appl. Phys. **111**, 054901 (2012).
[21]*Acoustic Metamaterials and Phononic Crystals*, edited by P. A. Deymier (Springer Science & Business Media, 2013), Vol. 173.
[22]X. Yan, R. Zhu, G. Huang, and F. Yuan, Appl. Phys. Lett. **103**, 121901 (2013).
[23]J. H. Sun and Yuan-Hai, in *2016 IEEE International Ultrasonics Symposium* (IEEE, 2016), Vol. 2, pp. 1–3.
[24]C. S. Park, Y. C. Shin, S. H. Jo, H. Yoon, W. Choi, B. D. Youn, and M. Kim, Nano Energy **57**, 327–337 (2019).

[25]C. J. Naify, T. P. Martin, C. N. Layman, M. Nicholas, A. L. Thangawng, D. C. Calvo, and G. J. Orris, Appl. Phys. Lett. **104**, 073505 (2014).
[26]J. Li, Z. Liu, and C. Qiu, Phys. Rev. B. **73**, 054302 (2006).
[27]A. Sukhovich, L. Jing, and J. H. Page, Phys. Rev. B **77**, 014301 (2008).
[28]L. Y. Zheng, Y. Wu, X. Ni, Z. G. Chen, M. H. Lu, and Y. F. Chen, Appl. Phys. Lett. **104**, 161904 (2014).
[29]J. Zhao, B. Bonello, L. Becerra, O. Boyko, and R. Marchal, Appl. Phys. Lett. **108**, 221905 (2016).
[30]S. Tol, F. L. Degertekin, and A. Erturk, Appl. Phys. Lett. **109**, 063902 (2016).
[31]V. Romero-García, A. Cebrecos, R. Picó, V. J. Sánchez-Morcillo, L. M. Garcia-Raffi, and J. V. Sánchez-Pérez, Appl. Phys. Lett. **103**, 264106 (2013).
[32]D. C. Calvo, A. L. Thangawng, M. Nicholas, and C. N. Layman, Appl. Phys. Lett. **107**, 014103 (2015).
[33]A. Allem, K. Sabra, and A. Erturk, Phys. Rev. Appl. **13**, 064064 (2020).
[34]Y. Jin, R. Kumar, O. Poncelet, O. Mondain-Monval, and T. Brunet, Nat. Commun. **10**, 143 (2019).
[35]S. C. S. Lin, T. J. Huang, J. H. Sun, and T. T. Wu, Phys. Rev. B. **79**, 094302 (2009).
[36]Z. Li, D. Wang, C. Fei, Z. Qiu, C. Hou, R. Wu, and Y. Yang, iScience **24**, 101988 (2021).
[37]B. Zhu, Y. Zhu, J. Yang, J. Ou-Yang, X. Yang, Y. Liand, and W. Wei, Sci. Rep. **6**, 39679 (2016).
[38]H. Salahshoor, M. G. Shapiro, and M. Ortiz, Appl. Phys. Lett. **117**, 033702 (2020).
[39]T. P. Martin, M. Nicholas, G. J. Orris, L. W. Cai, D. Torrent, and J. Sánchez-Dehesa, Appl. Phys. Lett. **97**, 113503 (2010).